Geophysical Journal International

Geophys. J. Int. (2018) **213,** 1804–1817
Advance Access publication 2018 February 28
GJI Geomagnetism, rock magnetism and palaeomagnetism

doi: 10.1093/gji/ggy077

Palaeomagnetic time and space constraints of the Early Cretaceous Rhenodanubian Flysch zone (Eastern Alps)

Edoardo Dallanave,[1] Uwe Kirscher,[2] Jürgen Hauck,[1] Reinhard Hesse,[1,3] Valerian Bachtadse[1] and Ulrich Georg Wortmann[4]

[1]*Department of Earth and Environmental Sciences, Ludwig Maximilians University, Theresienstrasse* 41, *Munich D*-80333, *Germany. E-mail: dallanave@geophysik.uni-muenchen.de*
[2]*Earth Dynamics Research Group, ARC Centre of Excellence for Core to Crust Fluid Systems (CCFS) and The Institute for Geoscience Research (TIGeR), Department of Applied Geology, WASM, Curtin University, GPO Box* U1987, *WA* 6845, *Perth, Australia*
[3]*Department of Earth and Planetary Sciences, McGill University,* 3450 *University St., Montréal, Québec H3A* 0E8, *Canada*
[4]*Department of Earth Sciences, University of Toronto,* 22 *Russel St., Toronto, Ontario M5S* 3B1, *Canada*

Accepted 2018 February 25. Received 2018 February 21; in original form 2017 May 31

SUMMARY

The Rhenodanubian Flysch zone (RDF) is a Lower Cretaceous–lower Palaeocene turbidite succession extending for ∼500 km from the Danube at Vienna to the Rhine Valley (Eastern Alps). It consists of calcareous and siliciclastic turbidite systems deposited in a trench abyssal plain. The age of deposition has been estimated through micropalaeontologic dating. However, palaeomagnetic studies constraining the age and the palaeolatitude of deposition of the RDF are still missing. Here, we present palaeomagnetic data from the Early Cretaceous Tristel and Rehbreingraben Formations of the RDF from two localities in the Bavarian Alps (Rehbrein Creek and Lainbach Valley, southern Germany), and from the stratigraphic equivalent of the Falknis Nappe (Liechtenstein). The quality of the palaeomagnetic signal has been assessed by either fold test (FT) or reversal test (RT). Sediments from the Falknis Nappe are characterized by a pervasive syntectonic magnetic overprint as tested by negative FT, and are thus excluded from the study. The sediments of the Rehbreingraben Formation at Rehbrein Creek, with positive RT, straddle magnetic polarity Chron M0r and the younger M′-1r′ reverse event, with an age of ∼127–123 Ma (late Barremian–early Aptian). At Lainbach Valley, no polarity reversals have been observed, but a positive FT gives confidence on the reliability of the data. The primary palaeomagnetic directions, after correction for inclination shallowing, allow to precisely constrain the depositional palaeolatitude of the Tristel and Rehbreingraben Formations around ∼28°N. In a palaeogeographic reconstruction of the Alpine Tethys at the Barremian/Aptian boundary, the RDF is located on the western margin of the Briançonnais terrain, which was separated from the European continent by the narrow Valais Ocean.

Key words: Magnetostratigraphy; Palaeomagnetism; Tectonics and landscape evolution.

1 INTRODUCTION

The Rhenodanubian Flysch zone (RDF), is an elongated belt of alternating Lower Cretaceous–lower Palaeocene turbidites and hemipelagic sediments with a maximum thickness of ∼1500 m. They crop out discontinuously for 500 km along the northern margin of the Eastern Alps, from the Danube Valley near Vienna (Austria) in the east to the Rhine Valley (Switzerland) in the west (Fig. 1; Hesse 2011). Constraining the age of deposition of the RDF has been a major geological problem for a long time. The RDF has been deposited in an abyssal plain below the calcite compensation depth (CCD, Hesse 1982; Mattern 1999; Wortmann *et al.* 1999), hampering good preservation of age diagnostic calcareous microfossils, and thus making precise biostratigraphy correlation difficult. Nevertheless, a number of studies were published since the 1960s, based on foraminifera, calcareous nannofossil and dinoflagellate cyst (dinocyst) biostratigraphy. These allow to constrain the age of the RDF from the Barremian in the Early Cretaceous to the Thanetian in the Palaeocene (Hesse 2011, and reference therein). This biostratigraphic dating is pinned by a carbon stable isotope-based correlation with reference records form Cismon (Italy) and the Vocotian Basin (SE France) (Wortmann *et al.* 2004; Fig. 2). Another geological issue is locating the allochthonous RDF in the palaeogeography of the evolving Tethys Ocean. In the Alpine stack of nappes, the RDF was thrust over the northern Ultrahelvetic and Helvetic domains (i.e. continental European margin) and overthrust by southern mélange units of an active margin (South Penninic) and by the Austroalpine units pertaining to the Adria plate

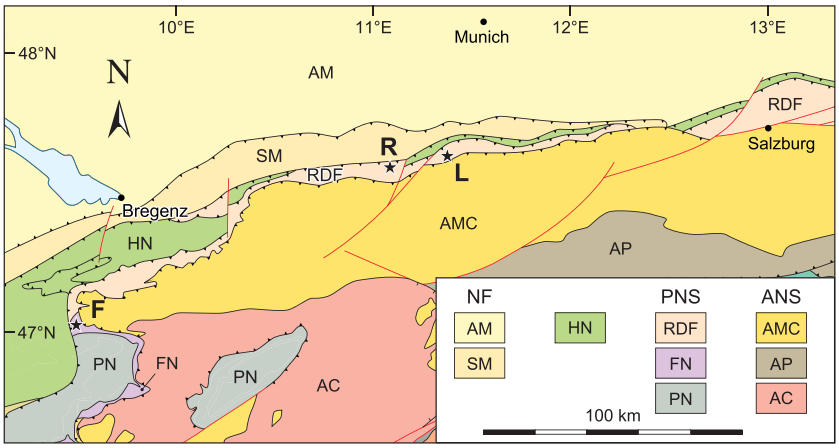

Figure 1. Simplified geological-tectonic map of the northeastern Alps (modified from Pfiffner 2014). NF = Northern Alps foreland (AM = Alpine Molasse; SM = Subalpine Molasse); HN = Helvetic and Ultrahelvetic nappes; PNS = Penninic Nappe system (RDF = Rhenodanubian Flysch zone; FN = Falknis Nappe; PN = other Penninic Nappes); ANS = Austroalpine Nappe system (AMC = Mesozoic cover; AP = Palaeozoic cover; AC = Crystalline basement). Palaeomagnetic sampling locations in the RDF are indicated by stars: (R) Hinterer Rehbrein Creek, 11°05′36″E, 47°37′40″N; (L) Lainbach Valley, 11°25′31″E, 47°42′02″N; (F) Falknis Nappe in Liechtenstein, 9°33′37”E, 47°04′26”N. The coordinates refer to the base of the sections.

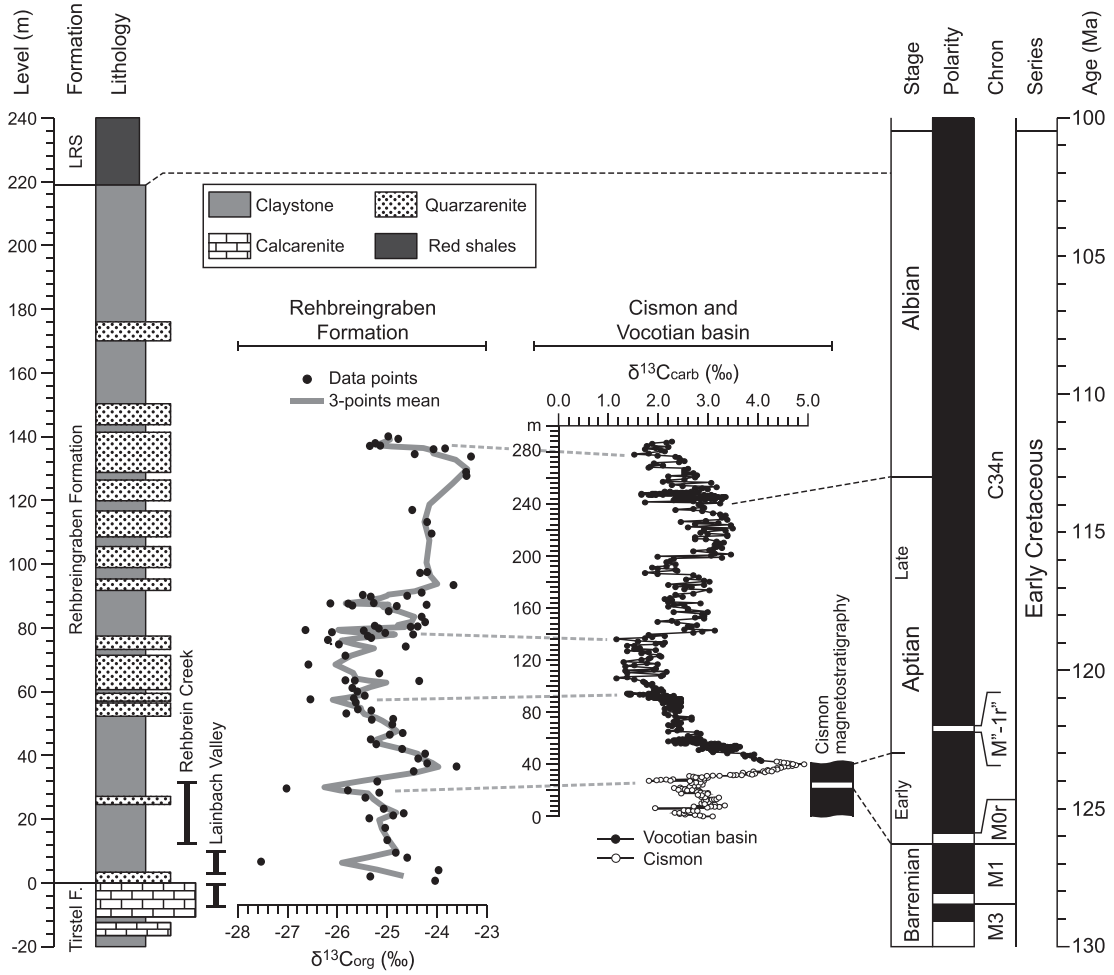

Figure 2. Stratigraphic column for the uppermost Tristel Formation, the Rehbreingraben Formation and the lower part of the Lower Red Shale (LRS). The lithological columns is represented together with the carbon isotope data from the same sediments and the correlation with the composite data set from the Vocotian Basin (SE France) and Cismon (Italy; modified from Wortmann *et al.* 2004), and the magnetic polarity stratigraphy from Cismon (Channell *et al.* 2000). The base of the LRS is biostratigraphically dated late Albian by Wagreich *et al.* (2006). The data set is correlated with the geomagnetic polarity timescale (GPTS) of Gradstein *et al.* (2012).

(Mattern 1999; Handy *et al.* 2010). Nonetheless, if the term Penninic and its north, middle and south subdivisions are convenient to distinguish the tectonic nappes in the Alpine geological context, its application to palaeogeographic domains is complicated by the fact that the vertical nappes stacking is not reflecting the original south to north palaeogeographic arrangement, but is affected by significant east–west transform motion, with lateral transport distances exceeding hundreds of kilometres (Wortmann *et al.* 2001; Handy *et al.* 2010). In fact, eastward motion of the European domains with respect Adria–Africa characterizes the early stage of the Alpine Orogeny during the Late Cretaceous (often referred to as Cretaceous orogeny). This is followed by a Cenozoic north–south-dominated compression causing nappes stacking and growth of the Alpine mountain range (Cenozoic orogeny; Pfiffner 2014). The RDF is commonly considered as deposited on the western margin of the Briançonnais terrane (Hesse 1973, 1974, 2011), a continental fragment separated from the European margin (*s.s.*) by the Valais Ocean. The Valais Ocean was a narrow (~100-km-wide) ocean branch, the opening of which began at the Jurassic–Cretaceous boundary (Handy *et al.* 2010). Many authors have questioned the existence of the Valais Ocean as a true oceanic basin (e.g. Mattern 1999). However, even if sediments attributed to the Valais palaeogeographic domain may not be floored by oceanic crust, there is evidence supporting mantle exhumation and seafloor spreading (Handy *et al.* 2010, and reference therein). Other authors have proposed a deposition of the RDF on the true European margin, that is, on the northwestern flank of the Valais–Piedmont Ocean (Egger *et al.* 2002).

In this study, we present palaeomagnetic data that allow precise correlation with the geomagnetic polarity timescale (GPTS12; Gradstein *et al.* 2012), significantly improving the age calibration of the Early Cretaceous part of the RDF. Palaeomagnetic directions are also used to constrain the palaeogeographic position of the RDF within the evolving Alpine Tethys. In addition, we present palaeomagnetic data from the Falknis Nappe of Liechtenstein, which are affected by synfolding remagnetization.

2 GEOLOGICAL SETTING

The RDF Supergroup is one of the five major palaeogeographic and tectonic units of the Northeastern Alps (Fig. 1). From north to south, they are (1) the Alpine Molasse Basin, the prototype of a retroarc or foreland basin, (2) the Helvetic and (3) Ultrahelvetic nappes, which represent the southern continental shelf and slope of Europe in Jurassic–Cretaceous and Early Tertiary time, (4) the Penninic nappe system, Including the RDF, commonly referred to as part of the Briançonnais–Valais Ocean domain, together with the Falkins and Tasna Nappes, and (5) the Northern Calcareous Alps or Austroalpine nappe, which represents the southern continental shelf belonging to the Adriatic plate.

In Bavaria, the RDF comprises a 1500-m-thick turbidite succession that was deposited from the Hauterivian–Barremian to the Maastrichtian (~130–70 Ma), that is, over a period of ~60 Myr. The RDF hosts sediments that were deposited by turbidity currents flowing, based on palaeocurrent indicators, parallel to the west–east basin axis, sometimes reversing flow directions during the life time of the basin (Hesse 1974, 1982). The RDF is divided in two facies, namely the Oberstdorf facies to the south, and the Sigiswang facies to the north, reflecting lithological lateral variations within the basin (Mattern 1999; Hesse 2011). In this study, we focus on the Lower Cretaceous uppermost Tristel Formation and the Rehbreingraben Formation (Hesse 1982) the latter often referred to in the literature as Flysch-Gault. These formations are part of the Obertsdorf facies; they were deposited by currents flowing uniformly from west to east and can be easily correlated over hundreds of kilometres parallel to the basin axis (Hesse 1973).

The Tristel Formation (Fig. 2) consists of up to 2-m-thick beds of turbiditic calcarenites interbedded with alternating layers of green and black claystone. Dinocyst biostratigraphy constrains the age of the Tristel Formation to the Barremian (Kirsch 2003). The calcarenites contain the full suite of turbidite structure divisions introduced by Bouma (1962), including grey marlstone at the top (T_e structure division). Light-coloured lutitic limestone thick up to 30 cm forms either separate beds or caps the calcarenite. Dark spots in the calcilutites are due to bioturbation. Whereas the carbonate-free claystone indicates deposition below the CCD, the calcarenites contain a high percentage of biogenic detritus. This consists of a rich shallow-water fauna of foraminifera ('miliolid' limestone), bryozoans, bivalves, gastropods and echinoderm fragments as well as subordinate algae (*Diplopora*). The detrital carbonate is allochthonous, deriving from a carbonate shelf source (Hesse 2011).

The Rehbreingraben Formation (Fig. 2) shows a marked lithologic contrast with respect to the underlying Tristel Formation. It consists of a siliciclastic succession of glauconitic carbonate-bearing quartzarenite alternating with black and green hemipelagic claystone, indicating a change of palaeoclimatic/palaeogeographic conditions. While the deposition of the Tristel Formation implies the presence of a tropical shelf as source of the carbonate detritus, the Rehbreingraben Formation was deposited under subtropical humid conditions with weathering of the basement beneath the carbonate platform, suggesting at least partial erosion of the carbonate cover (Wortmann *et al.* 2004). The average thickness of individual quartzarenitic turbidite beds is 1 m, reaching a maximum of ~4 m. They commonly contain turbidite structure divisions T_b (parallel lamination), T_c (ripple-cross lamination and convolute lamination) and T_d (parallel and convolute lamination) of Bouma (1962). Thin caps of grey marlstone generally not exceeding 20 cm in thickness represent the pelitic division T_e. The green and black carbonate-free/carbonate-poor claystone were deposited under suboxic to anoxic conditions, respectively (Wortmann *et al.* 1999). Organic carbon concentrations in the black claystone reach up to 6 per cent by weight but remain below 1 per cent in the green claystone. Based on geochemical analyses, Wortmann *et al.* (1999) interpreted the black–green rhythms as palaeoclimatically controlled, likely related to precessional cycles. The formation has been stratigraphically subdivided at the strata level as it is possible to correlate detailed measured sections of the Rehbreingraben Formation bed-by-bed over a distance of 115 km between the Iller river to the west and Lake Tegernsee to the east (Hesse 1973, 1974), making it the stratigraphically best-subdivided unit of the RDF. The thickness of the Rehbreingraben Formation reaches 225 m in the completely exposed section of the 'Hinterer Rehbreingraben' near Unterammergau (Hesse 2011, Fig. 2). Recent biostratigraphic data from the Lower Red Shales (in the literature also referred to as 'Untere Bunte Tonsteine'), which overly conformably the Rehbreingraben Formation, constrain the stratigraphic top of the latter to the late Albian (Wagreich *et al.* 2006).

3 MATERIALS AND METHODS

A total of 296 standard palaeomagnetic samples were collected from two localities within the RDF between the Iller River and Lake Tegernsee, ~50 km to the south of Munich. They are (i) the Hinterer Rehbrein Creek (hereafter referred to as Rehbrein Creek)

and (ii) the Lainbach Valley, both exposing part of the Lower Cretaceous stratigraphic series (Fig. 1). At Rehbrein Creek, 187 samples were collected along a ∼20-m-thick section of alternating black and green shales, and quartz-rich turbidites from the base of the Rehbreingraben Formation. Samples strata dip ∼80° to the SSW (∼190°). In the Lainbach Valley, 67 samples were obtained from the Rehbreingraben Formation and another 42 from the Tristel Formation. Here, the samples were collected on the two limbs of a fold, with strata, respectively, dipping toward 162° by 63°, and toward 353° by 78°. In the Eastern Alps, fold hinges are generally oriented roughly E-W as a consequence of the Cenozoic Alpine orogeny N-S compression (Pfiffner 2014). Another 15 samples for palaeomagnetic analysis were collected from two sections in the Falknis Nappe in Liechtenstein (Fig. 1), the first in the stratigraphic equivalent of the Tristel Formation of the RDF at the proximal end of the joint depositional system, the second in Neokom Flysch, which stratigraphically underlies the Tristel Formation. Samples from the Tristel Formation (equivalent) have been here collected on the two limbs of an overturned fold, with a dip direction/dip for the two limbs of respectively 80°/23° and 216°/66°, the latter overturned. Strata belonging to the Neokom Flysch also crop out on the two limbs of an overturned fold, plunging respectively toward 125° by 46°, and 170° by 66° (overturned).

Samples consist of standard palaeomagnetic cores of 2.54 cm of diameter, taken with a gasoline-powered drill and oriented with a magnetic compass. From each core, a standard ∼11 cm^3 specimen for palaeomagnetic analyses has been trimmed. The specimens were subjected to both alternating field (AF; 247 specimens) and thermal (67 specimens) stepwise demagnetization, with peak fields of 150 mT and maximum temperatures of ∼600 °C, respectively. The natural remanent magnetization (NRM) has been measured after each demagnetization step with a *2-G Enterprises* SQUID magnetometer located in a magnetically shielded room. Specimens were demagnetized using a *2-G Enterprises* AF demagnetizer and a *Schonstedt* thermal demagnetizer. The vector components of the NRM were isolated by means of principal component analysis of Kirschvink (1980) interpolating at least six consecutive demagnetization steps. The average directions and associated statistical parameters were calculated using the spherical statistics of Fisher (1953).

We used a set of representative specimens from the Rehbrein Creek and Leinbach Valley to investigate the magnetic mineralogy content of the sediments. Stepwise isothermal remanent magnetization (IRM) acquisition curves (up to 1.6 T) were obtained using a *MMPM 10 Pulse Magnetizer*. Thermomagnetic remanence analysis was performed gradually heating samples up to 700 °C in an inducing field of 800 mT with a *variable field translation balance* (*Petersen Instruments*) in either air or nitrogen atmosphere.

Anisotropy of magnetic susceptibility (AMS) was measured following the 15 positions protocol of Jelínek (1978) on 34 specimens from the Rehbrein Creek and 5 from the Lainbach Valley. Measurements were performed with a *KLY-2 Kappabridge* from *AGICO*. All analyses were conducted at the palaeomagnetic laboratory of the Ludwig Maximilians University of Munich (Germany).

4 RESULTS

4.1 Rehbrein Creek and Lainbach Valley

4.1.1 Rock magnetism

The IRM acquisition curves of samples from the Tristel Formation and the Rehbreingraben Formation (Fig. 3a) show a steep increase of magnetization up to ∼200 mT, the field at which they reach saturation.This behaviour indicates the exclusive presence of low coercivity magnetic phases. Thermomagnetic remanence curves, when performed in air (i.e. oxidizing environment), show two behaviours. The first is characterized by a decrease of intensity reaching zero at ∼580 °C, in agreement with the presence of magnetite (Figs 3b and c). In the second, the magnetization is characterized, after a decrease up to ∼450 °C, by a variable 'hump' centred at ∼510 °C and decreasing to zero at ∼580 °C (Figs 3d and e, cycle 1). This can be related to the formation of magnetite during heating from a ferriferous precursor (Hirt *et al.* 1993), leading to a post cooling magnetization that is up to five times higher than before heating. Repeated experiments on the same specimen tend to increase the final Curie temperature up to >600 °C, indicating the formation of haematite (Fig. 3e, cycles 3–5). When the experiments are performed in nitrogen (i.e. non-oxidizing) atmosphere (Fig. 3f), the cooling branch of cycle 1 shows a remarkable increase of magnetization at 300 °C, in agreement with the presence of paramagnetic pyrite irreversibly turning to ferromagnetic pyrrhotite (Wang *et al.* 2008). Repeated experiment led to the formation of magnetite, as indicated by the measured Curie temperature of ∼580 °C (Fig. 3f, cycle 2). These data fit with the pyrite $\overset{1}{\rightarrow}$ pyrrhotite$\overset{2}{\rightarrow}$ magnetite $\overset{3}{\rightarrow}$ haematite pathway observed in repeated thermomagnetic experiments of natural crystalline pyrite (Wang *et al.* 2008). Under nitrogen atmosphere, the overall process is slowed down, resulting in a high relative concentration of pyrrhotite at the end of cycle 1.

4.1.2 Anisotropy of magnetic susceptibility

Results of the AMS analyses are show in Fig. 4. After correction of bedding tilt, in both Rehbrein Creek and Lainbach valley the minimum axes (k_3) of the AMS tensor is oriented vertically, while the maximum (k_1) and the intermediate (k_2) lie horizontally, parallel to the bedding plane (Figs 4a and b). At Rehbrein Creek, the number of data is high enough to evaluate the orientation of the average tensor through the bootstrap approach of Constable & Tauxe (1990; Fig. 4c and Table S1, Supporting Information). This analysis also suggests an oblate shape of the average tensor, with overlapping k_1 and k_2 confidence ellipses (Table S1, Supporting Information). At Lainbach, we calculate the orientation of the AMS tensor using the statistic of (Jelínek 1978; Fig. 4b). Data from both the localities have been compared using the corrected anisotropy degree (P') and the shape factor (T) of Jelínek (1981):

$$P' = \exp\sqrt{\{2\left[(\eta_1-\eta)^2+(\eta_2-\eta)^2+(\eta_3-\eta)^2\right]\}}$$

$$T = \frac{2\eta_2-\eta_1-\eta_3}{\eta_1-\eta_3}$$

where η_1, η_2 and η_3 the natural logarithm of k_1, k_2 and k_3, and $\eta = (\eta_1+\eta_1+\eta_3)/3$.

Data from Rehbrein Creek are characterized by a higher degree of anisotropy, with an average value of $P' = 1.1$ and peak values of 1.15 (Fig 4d and Table S1, Supporting Information). Associated positive values of T indicate that the anisotropy is dominated by oblate shape (Jelínek 1981), in agreement with the bootstrap analysis. This fabric is typical of compacted sediments not affected by tectonic deformation (Parés *et al.* 1999). At Lainbach, the shape factor T shows both positive and negative values, but P'- has an average value of 1.01, indicating very weak (∼1 per cent) anisotropy of the AMS tensor (Martín-Hernández *et al.* 2004; Cifelli *et al.* 2005, Table S1, Supporting Information). The maximum eigenvector k_1 is however

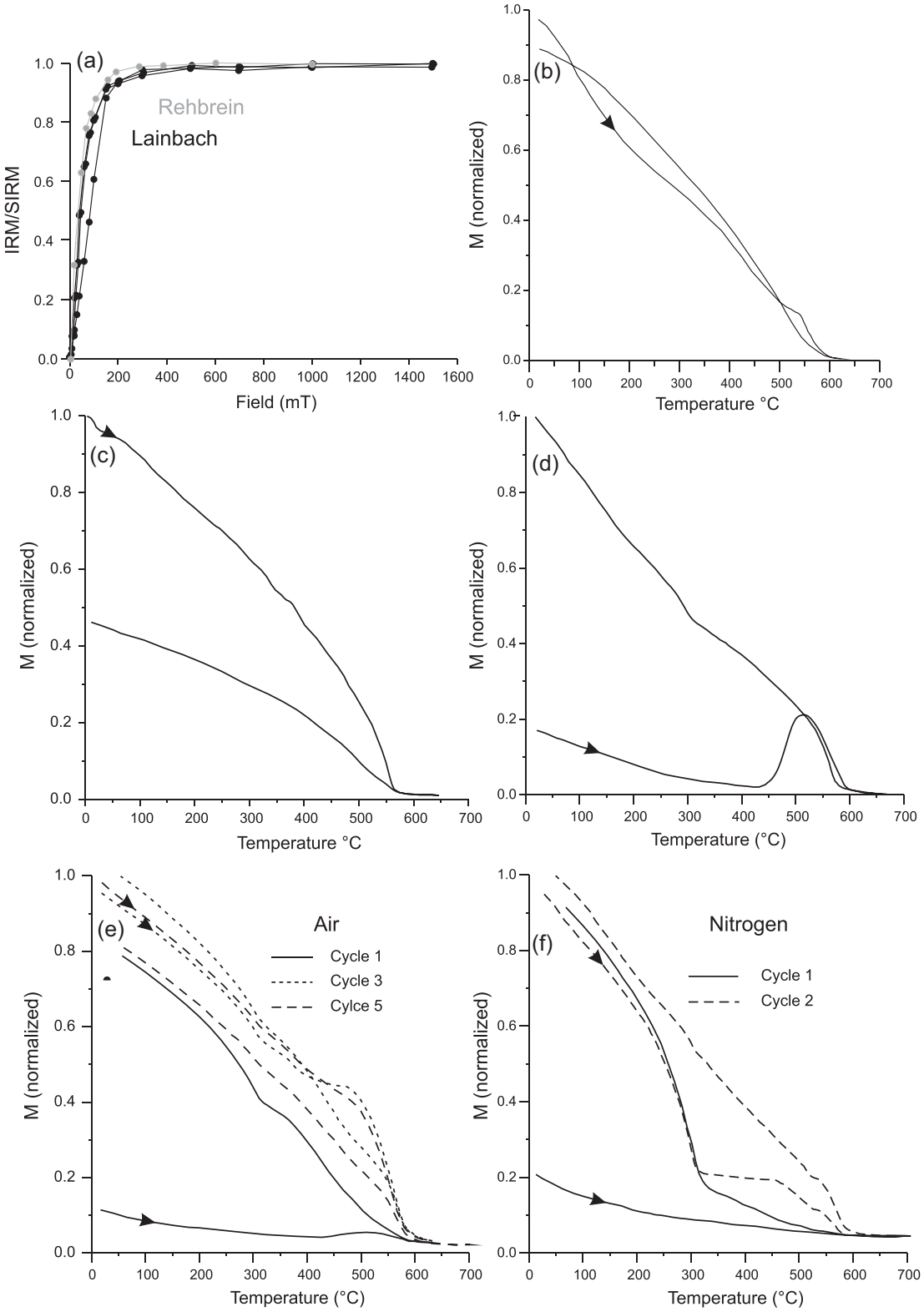

Figure 3. (a) IRM acquisition curves for samples from the Rehbrein Creek (grey) and Lainbach Valley (black) sections. (b)–(d) Representative thermomagnetic remanence curves of specimens from Lainbach Valley; arrows indicate the heating cycle. (e) and (f) Examples of repeated thermomagnetic remanence curves from Rehbrein Creek performed in oxidizing (air) and nitrogen atmosphere; arrows as in (b)–(d).

oriented WSW (Fig 4b and Table S1, Supporting Information). This orientation can possibly be related to clay particles orientation in the sediments, reflecting the directions of the turbidity currents, as indicated also by geological evidence (Hesse 1965, 1982, 2011). We cannot rule out the possible effect of a post depositional tectonic deformation on the shape of the AMS tensor. However, with such low P' values, we can reasonably exclude any possible influence on the orientation of the characteristic remanent directions.

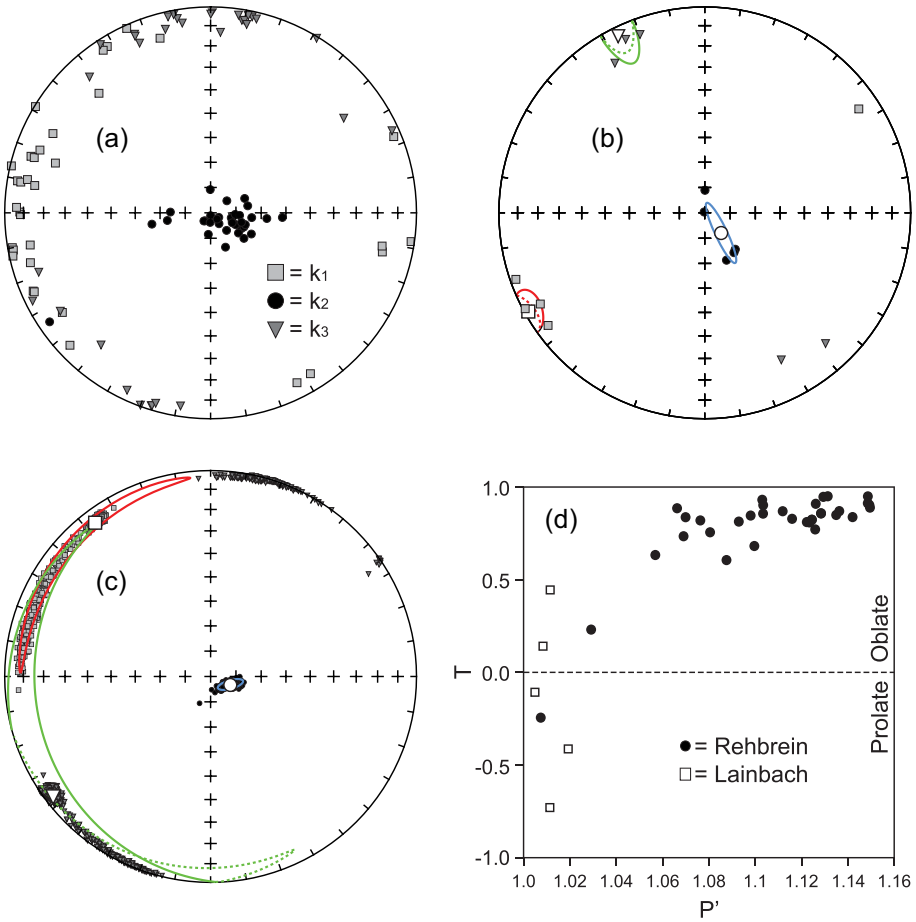

Figure 4. Stereographic plot of the axes (k_1, k_2 and k_3) of the anisotropy of magnetic susceptibility (AMS) tensor for samples from Rehbrein Creek (a) and Lainbach Valley (b) after correction of bedding tilt. (c) Bootstrap analysis (Constable & Tauxe 1990) of AMS data from Rehbrein Creek, a derived confidence ellipses. (d) Plot of the corrected anisotropy degree (P') versus shape factor (T) of Jelínek (1981) for both Rehbrein Creek and Lainbach Valley. Data used are listed in Table S1 in the Supporting Information.

4.1.3 Palaeomagnetism

In general, both AF and thermal demagnetization experiments yield good and comparable results (Fig. 5). The 88 per cent of the specimen from Rehbrein Creek were characterized by stable behaviour. The 60 and 90 per cent of the samples from, respectively, the Rehbreingraben and Tristel formations in the Lainbach Valley show also stable demagnetization behaviour. The specimens are characterized by the presence of two components of the NRM. A spurious low temperature (or coercivity) component is removed completely after heating to ∼300 °C (or after peak AF of ∼20 mT). After removal of this overprint, a characteristic remanent magnetization (ChRM) component linearly trending towards the origin of the orthogonal projection has been unblocked at peak temperatures of ∼550 °C and AF of ∼120 mT. These results are discussed for the two sampling localities as follows.

Rehbrein Creek. Pilot thermal demagnetization revealed that the specimens were going through disaggregation during heating. They were however successfully treated with AF demagnetization (Figs 5a and b), isolating 151 ChRM directions on 187 samples (∼81 per cent). Directions are organized in two modes that, after correction for bedding tilt, point NNE-and-down and SSW-and-up (Figs 6a and b). The average directions of the two tilt corrected modes depart from antipodality by 13.6°, passing the reversal test (RT) of Watson (1983; $V_w = 5.7$, $V_{critical} = 6.2$; see also Tauxe 2010 for details), with an assigned class 'C' of McFadden & McElhinny (1990). Average directions and associated statistical parameters of Fisher (1953) are listed in Table 1.

We calculated the position of the virtual geomagnetic pole (VGP) associated with each ChRM direction. The latitude of VGPs relative to the mean palaeomagnetic (north) pole has been used to determine the magnetic polarity across the section. Positive (negative) VGP latitudes are considered as representative of normal (reverse) magnetic field polarity. The section is generally dominated by normal polarity, with one ∼1.1-m-thick reverse interval centred at 8.4 m, plus three minor reverse levels (based on at least two specimens) of about 0.2, 0.2 and 0.3 m and centred, respectively, at 12.6, 13.7 and 19.0 m levels (Fig. 7).

Sedimentary rocks can be affected by inclination flattening of palaeomagnetic directions of different magnitude, and the amount of flattening depends on both the magnetic carrier and the degree of post-depositional compaction (King 1955; Tauxe & Kent 1984; Anson & Kodama 1987; Tan *et al.* 2002). In order to detect and correct for inclination shallowing, Tauxe & Kent (2004) developed a statistical method based on the expected shape of the palaeomagnetic directions distribution. It consists of progressively unflattening the directions by decreasing the flattening parameter 'f' (King 1955) within the formula $\tan I_f = f \tan I_0$ (where I_f and I_0 are the measured inclination and the true inclination of the geomagnetic field during

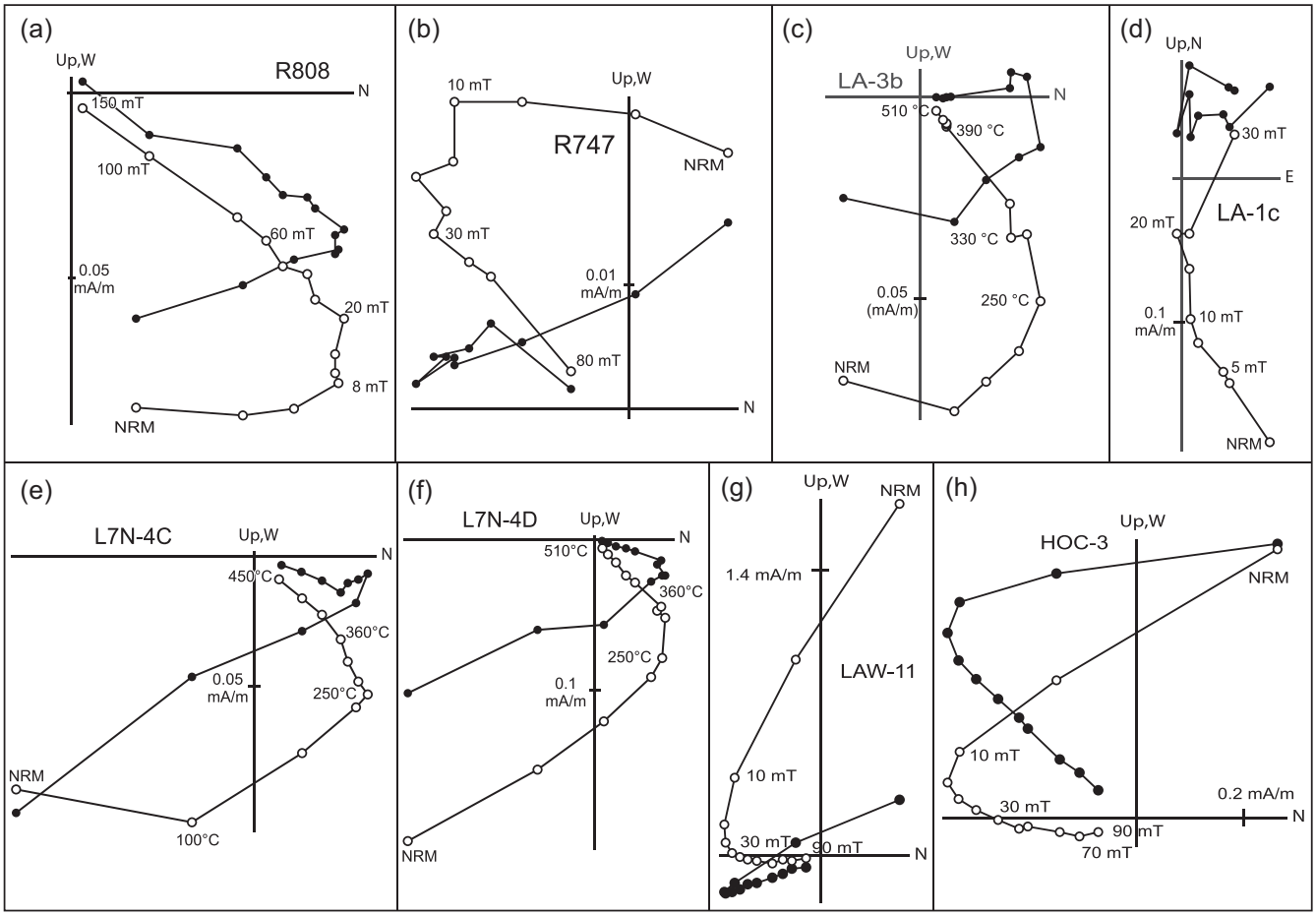

Figure 5. Representative orthogonal vector endpoints demagnetization diagrams (Zijderveld 1967), shown in bedding tilt corrected coordinates, from representative samples (a) and (b) from the Rehbreingraben Formation at Rehbrein Creek, (c) and (d) from the Rehbreingraben Formation, (e) and (f) the Tristel formation at Lainbach Valley and (g) and (h) from the Falknis Nappe in Liechtenstein. Solid and open dots represent vector endpoints projected onto the horizontal and vertical planes, respectively.

sedimentation, respectively) until the distribution shape assume an *E*/*I* pair of values that is consistent with the TK03.GAD field model (Tauxe & Kent 2004). The *E*/*I* method has been successfully applied to several sediments of different age (Dallanave *et al.* 2012a; Muttoni *et al.* 2013; Kirscher *et al.* 2014). Since ChRM directions with associated VGP latitude comprises between 45°N and 45°S can be considered as transitional, that is, not reflecting the long-term behaviour of the geomagnetic field (McElhinny & McFadden 1997), we filtered the Rehbrein Creek data set eliminating directions falling in this category (Fig. 6b). The filtered data set (VGP_{45}) results in 133 directions with the two polarity modes passing the Watson's RT ($V_w = 6.2$, $V_{critical} = 6.6$; departure form antipodality = 10.9°). Applying the correction to the VGP_{45} directions, they match the *E*/*I* pair of values predicted by the TK03.GAD model after reaching a flattening factor $f = 0.44$, not unusually high for compacted sediments (e.g. Dallanave *et al.* 2009; Muttoni *et al.* 2013). We estimated the 95 per cent uncertainty of the correction repeating the analyses with 5000 bootstrapped data set (Tauxe *et al.* 2016). This results in an unflattened inclination of 43.7° (Fig. 6c and Table 1), that is, 19.5° steeper than the original.

The TK03.GAD model predicts circular VGP distributions from sites at all latitudes. We therefore assessed the robustness of the *E*/*I* analyses calculating the circular symmetry of the VGP distribution before and after shallow bias correction with the quantile–quantile (Q-Q) analyses proposed by Tauxe (2010). VGPs circular uniformity has been evaluated through a Kolmogorov–Smirnov based M_u test (Fisher *et al.* 1987; Tauxe 2010). The null hypothesis of uniformity cannot be rejected at 90 per cent level of confidence only after *E*/*I* correction (Fig. 8a). The palaeomagnetic poles obtained from the VGP_{45} set of directions before (R1) and after (R2) *E*/*I* correction are shown in Fig. 8(b) (Table 2).

Lainbach Valley. In the Lainbach Valley, sediments pertaining to the Tristel Formation and the Rehbreingraben Formation were initially analysed separately. A pilot demagnetization phase on the Lainbach sediments revealed that thermal demagnetization is more effective (Figs 5c–f) and it was thus adopted. A total of 87 ChRM directions were obtained from 109 samples (80 per cent), 45 from the Rehbreingraben Formation and 42 from the Tristel Formation. At both sites, the samples were collected on the two limbs of a fold (see above), and the ChRM directions are organized in two distinct modes that converge after correction for bedding tilt (Figs 6d–g and Table 1). Performing the fold test (FT) of Enkin (2003), the maximum *k* value is reached at an unfolding level of 93.9 ± 5.1 per cent for the Rehbreingraben Formation and 97.8 ± 4.9 per cent for the Tristel Formation, respectively (Figs 6h and i). These results indicate a pre-folding (likely primary) acquisition of the ChRM component. Since the resulting tilt corrected mean directions are reciprocally contained in the α_{95} cone of confidence (inset in Fig. 6g) and the two formations are similar in age, we combine the ChRM directions after tilt correction (Table 1). We used the

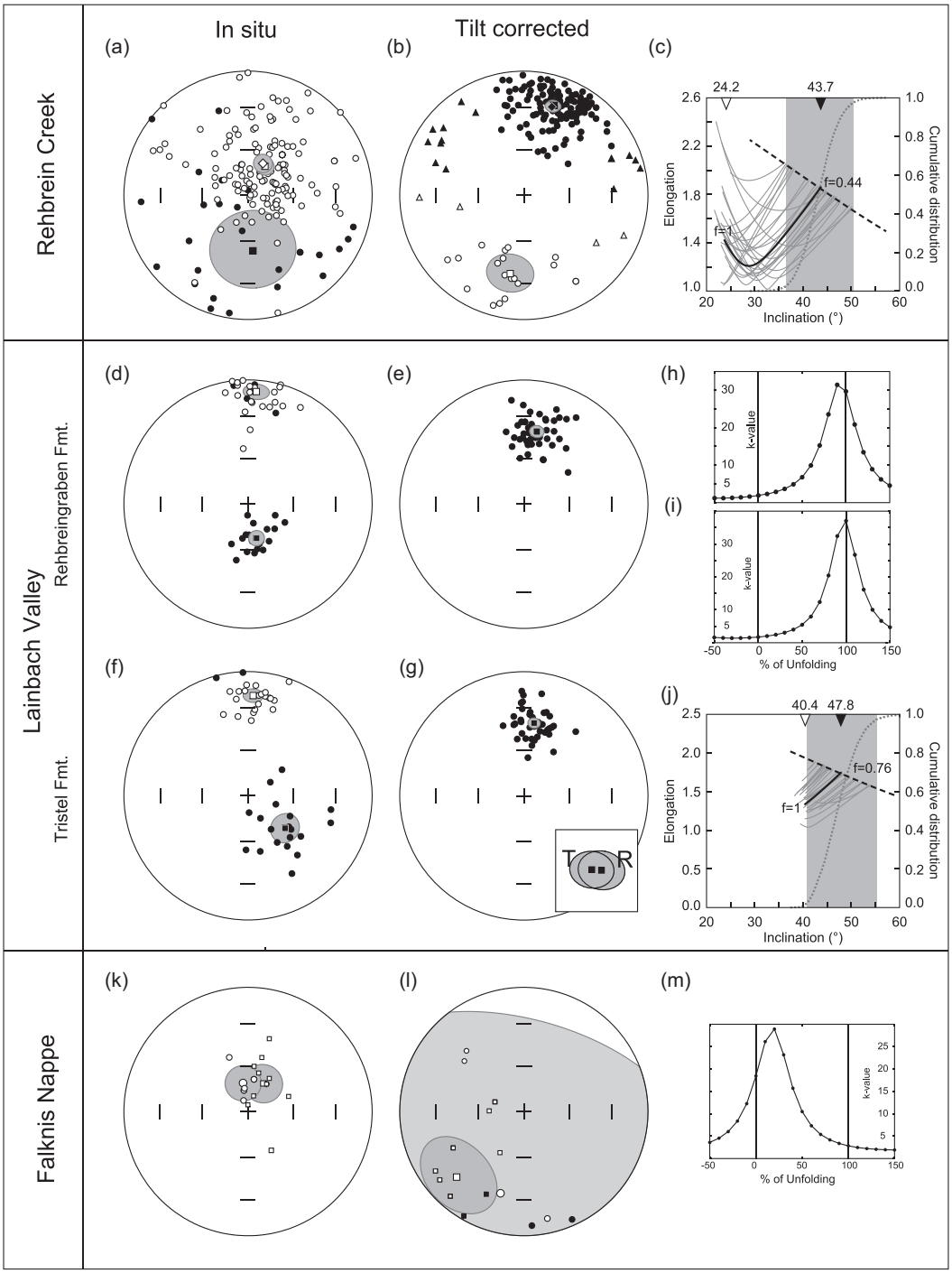

Figure 6. Equal-area projection of the characteristic remanent (ChRM) directions from the Rehbreingraben Formation at Rehbrein Creek in *in situ* (a) and tilt corrected (b) coordinates. Open (closed) dots represent up- (down-) pointing directions, squares represent the mean directions with associated α_{95} confidence boundaries (Fisher 1953), while the diamond is the average direction plotting all ChRM direction to a common down-pointing polarity; triangles are ChRM directions not included in the set used for the inclination flattening correction as explained in the main text. (c) Elongation versus inclination (*E*/*I*) analyses (Tauxe & Kent 2004; Tauxe *et al.* 2016) result of selected ChRM directions from Rehbrein Creek; the solid black line is the trajectory of *E*/*I* calculated after applying flattening factor (*f*; King 1955) ranging from 1.0 to 0.42. At 0.42 data fit, the TK03.GAD predicted *E*/*I* value (dashed black line). Solid grey lines are 25 examples of the 5000 bootstrapped data sets on which the same *E*/*I* analysis has been performed. Results from the bootstrapped data set are added in a normalized cumulative distribution (dotted grey line) that was used to estimate the 95 per cent confidence boundaries (grey band). Mean inclination before (open triangle) and after (closed triangle) *E*/*I* correction are shown on top of the diagram. The ChRM directions from Lainbach Valley are shown for the (d) and (e) Rehbreingraben Formation and (f and g; symbols as above) Tristel Formation; the mean directions from the two formations are statistically undistinguishable (inset in panel 'g'). Precision parameter '*k*' (Fisher 1953) versus percentage of unfolding is shown for data from the (h) Rehbreingraben Formation and (i) Tristel Formation. (j) The *E*/*I* test as described above has been performed with the combined data set. ChRM directions from the Falknis Nappe (Liechtenstein) are shown (k) before and (l) after tilt correction; circles are directions from the Tristel Formation (equivalent), while squares are directions from the Neokom Flysch; bigger symbols are average directions with associated 95 per cent cone of confidence; dispersion of the data increases with unfolding (m) suggesting the presence of a syn- (or post-) folding pervasive magnetic overprint.

Table 1. Average characteristic remanent magnetization (ChRM) directions.

		Geographic (*in situ*) coordinates				Bedding (tilt-corrected) coordinates			
N	MAD	*k*	α_{95}	DEC	INC	*k*	α_{95}	DEC	INC (INC*)
Hinterer Rehbrein Creek									
Mode 1 (Reverse polarity)									
22	6.2 ± 4.0	2.2	27.0	174.9	53.0	5.7	13.9	190.0	−36.2
Mode 2 (Normal polarity)									
129	5.2 ± 3.4	4.9	5.9	30.3	−67.9	9.8	4.0	18.5	24.7
Mode 1 + 2									
151	5.3 ± 3.5	4.2	6.1	25.1	−66.9	8.8	3.9	17.6	26.2
Hinterer Rehbrein Creek, VGP_{45} directions									
Mode 1									
18	7.1 ± 4.3	–	–	–	–	10.3	10.7	199.8	−33.5
Mode 2									
115	5.3 ± 3.5	–	–	–	–	17.4	3.3	19.1	22.6
Mode 1 + 2									
133	5.5 ± 3.6	–	–	–	–	15.4	3.2	19.2	24.2 ($43.7^{50.4}_{36.4}$)
Lainbach Valley, Rehbreingraben Formation									
Mode 1									
26	9.6 ± 5.5	19.4	6.6	4.2	−10.1	27.1	5.5	12.5	43.7
Mode 2									
19	7.0 ± 5.0	44.1	5.1	166.0	66.9	43.9	5.1	7.2	35.6
Mode 1 + 2									
45	8.5 ± 5.4	–	–	–	–	30.1	3.9	10.1	40.3
Lainbach Valley, Tristel Formation									
Mode 1									
19	7.7 ± 3.8	13.4	9.5	131.2	57.4	32.4	6.0	7.7	38.2
Mode 2									
23	8.0 ± 5.4	32.6	5.4	2.9	−20.3	42.0	4.7	8.3	42.4
Mode 1 + 2									
42	7.8 ± 4.7	–	–	–	–	37.1	3.7	8.0	40.5
Lainbach Valley, Tristel and Rehbreingraben Formations									
87	8.2 ± 5.1	–	–	–	–	33.4	2.7	9.1	40.4 ($47.8^{55.3}_{40.9}$)
Falknis Nappe, Tristel Formation (equivalent)									
5	4.4 ± 0.5	15.4	12.7	28.4	−69.1	4.8	24.6	225.7	−25.4
Falknis Nappe, NeokomFlysch									
9	7.3 ± 2.7	43.7	11.7	350.2	−71.1	1.4	120.7	196.0	−32.2

combine data set to perform an *E*/*I* test as described for Rehbrein Creek. The distribution of ChRM directions from Lainbach matches the TK03.GAD predicted *E*/*I* values applying a flattening factor $f = 0.76$ (Fig. 6j). Value of '*f*' around 0.8 are commonly observed in sediments (Muttoni *et al.* 2013, and reference therein). It is however considerably higher than the $f = 0.44$ estimated ad Rehbrein Creek. Differences in the degree of inclination shallowing in sediments can have multiple sources, varying from the mineralogical content (i.e. quartz versus clay minerals) to the post-depositional processes. For example, coeval early Eocene clay-rich sediments belonging to the same formation and exposed in two nearby localities of the venetian southern Alps, have an estimated *f* factor of 0.35 and 0.14, respectively (Dallanave *et al.* 2012b). The average degree of AMS (P') at Rehbrein Creek is 1.1, while at Lainbach P' is systematically lower than 1.02. This indicates a higher degree of compaction of the Rehbrein Creek sediments, thus justifying the higher degree of inclination shallowing. This likely derives from the higher clay content of the sediments at Rehbrein Creek.

Also for the combined Lainbach Valley data set we estimated the circular symmetry of the VGPs before and after correction by means of Q-Q analyses. The applied correction of $f = 0.76$ does indeed improve the circularity of the distribution, the uniformity of which cannot be rejected at 90 per cent level of confidence only after *E*/*I* correction (Fig. 8c). The palaeomagnetic pole before (L1) and after (L2) unflattening correction is shown in Fig. 8(b) (Table 2).

4.2 Falknis Nappe

The strata of the Tristel Formation (equivalent) and the Neokom Flysch sampled in Liechtenstein are, in both cases, deformed by multiple folding phases. Demagnetization diagrams obtained using AF cleaning yield stable behaviour (Figs 5g and h), well grouped in *in situ* coordinates (Fig. 6k). However, after correction for bedding tilt the ChRM directions disperse and the precision parameter *k* decreases dramatically at both sites (Fig. 6l). The ChRM directions from the two sections were combined and analysed with a parametric FT (Watson & Enkin 1993). The FT suggests an acquisition of the ChRM at 18 per cent (±1.8 per cent) of unfolding (Fig. 6m). Pervasive shearing parallel to the fold-axis planes might have provided access to advected pore fluids that could have altered the magnetic phases. The complex folding history makes any correlation

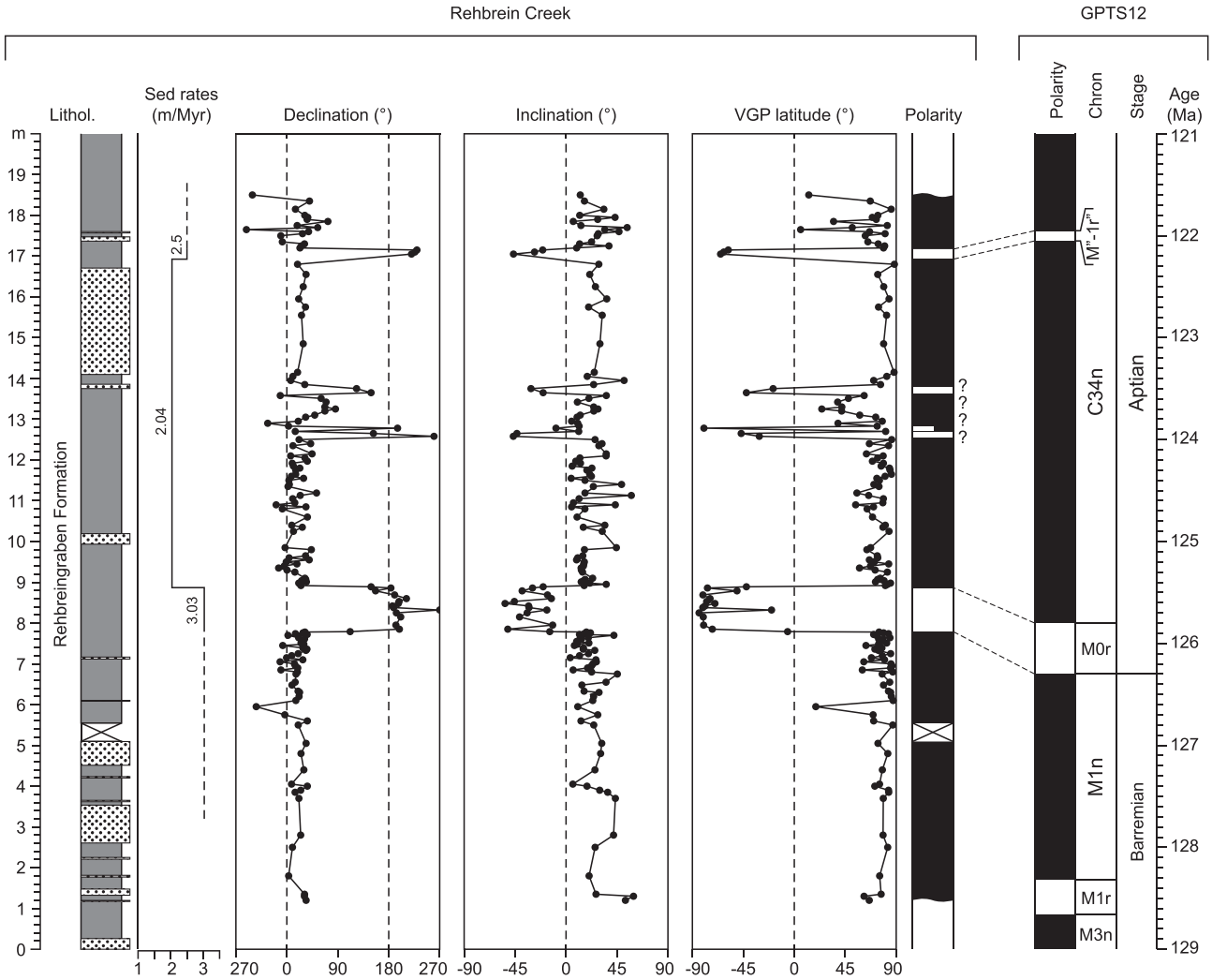

Figure 7. Magnetic polarity stratigraphy of the Rehbrein Creek section and correlation with the geomagnetic polarity timescale of Gradstein *et al.* (2012; GPTS12). From left to right: simplified lithological column (symbols as in Fig. 2) with thickness and sedimentation rates, calculated by means of magnetostratigraphic correlation with the GPTS12; declination and inclination of the characteristic remanent (ChRM) directions with associated virtual geomagnetic poles (VGPs) latitude, calculated with respect the average palaeomagnetic (north) pole; magnetic polarity stratigraphy, derived by the zero-crossing points of the VGP latitude curve; correlative part of the GPTS12.

of this direction with published palaeomagnetic poles difficult and not reliable (see Kirscher *et al.* 2013 for a discussion). Due to the synfolding nature of the ChRM, no further analyses have been conducted on the samples from the Falknis Nappe and the results are not further considered.

5 DISCUSSION

5.1 Magnetostratigraphy and age model

Dinoflagellate cyst biostratigraphy (Kirsch 2003) indicates a late Barremian–early Aptian age for the base of the Rehbreingraben Formation. A good uppermost Albian age constrain for the top of the Rehbreingraben Formation is given by integrated dinocyst, calcareous nannofossil and planktic foraminifera biostratigraphy (Wagreich *et al.* 2006). This age assignment is underpinned by a carbon stable isotope-based correlation with the reference $\partial^{13}C$ compilation from Cismon (Italy) and the Vocontian Basin (SE France; Wortmann *et al.* 2004). This biochemostratigraphic constraint allows correlating the 1.1-m-thick reverse polarity zone at 7.8 in the Rehbrein Creek section with the M0r magnetic polarity Chron of the GPTS (Fig. 7). This reliable correlation implies a sedimentation rate for this part of the section of 3.03 m Myr^{-1}. Among the brief reverse polarity events observed during Chron C34n (Cretaceous Normal Polarity Superchron), the oldest and best established is the M′-1r′, often referred to as ISEA reverse event, and observed in both deep-sea and outcropping sediments (Vandenberg et al. 1978; Tarduno 1990; Tarduno *et al.* 1989), as well as in volcanic rocks (Zhu *et al.* 2004). We correlate the ∼0.25 m reverse interval observed at ∼17 m at Rehbrein Creek with this event. This is the most reliable correlation for two reasons. First, this interval is based on three ChRM directions and thus more robust. Second, the average sedimentation rates determined by this correlation (2.13 m Myr^{-1}) are very similar the ones expected by the $\partial^{13}C$-based correlation of Wortmann *et al.* (2004) for this formation (∼2.4 m Myr^{-1}). Correlating the two sample-based short reverse intervals observed at about ∼13 and 14 m with the M′-1r′event would result in unreasonably low sedimentation rates (<1 m Myr^{-1}). Between M0 and M′-1r′,

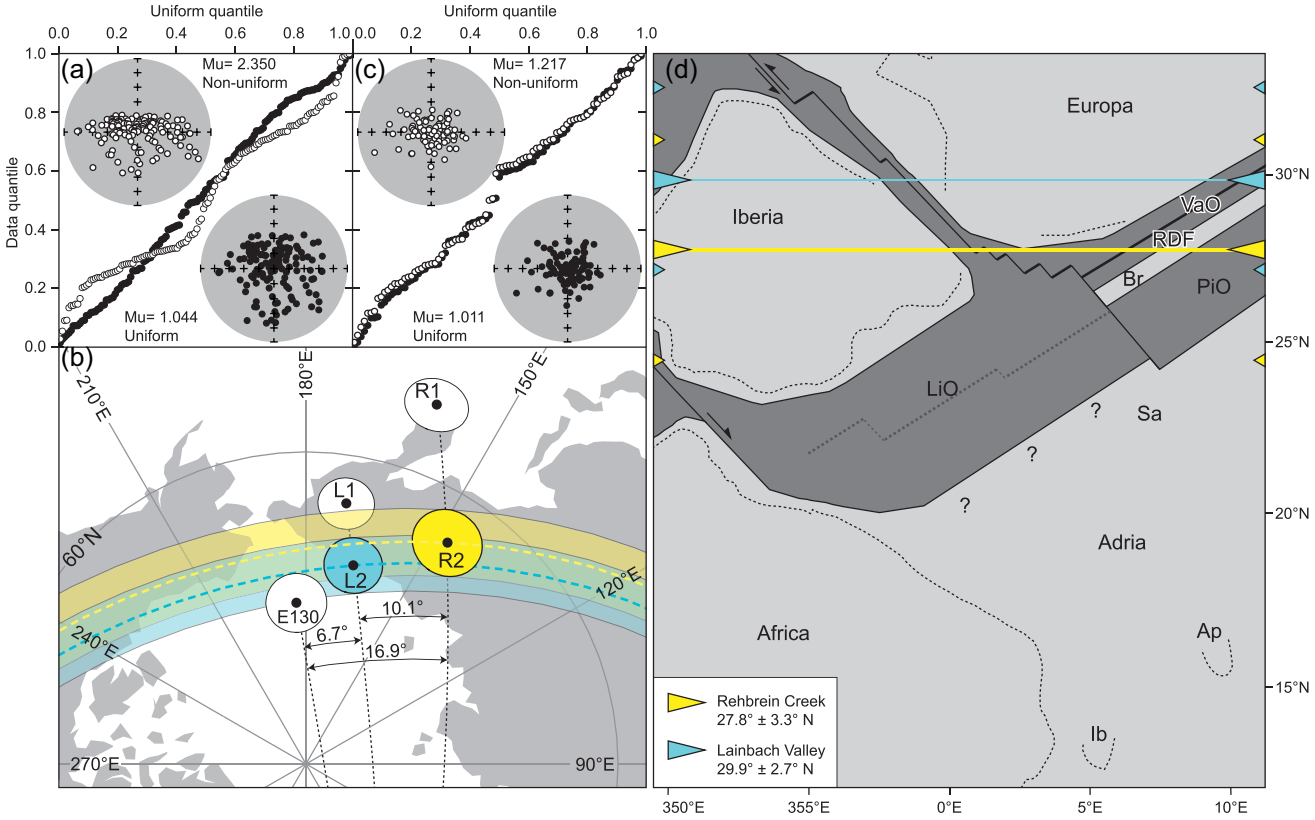

Figure 8. (a) Quantile–quantile (Q-Q) analyses for the virtual geomagnetic poles (VGPs) from Rehbrein Creek before (open dots) and after (closed dots) elongation versus inclination (*E*/*I*) correction for inclination shallowing of palaeomagnetic directions; a uniform distribution of VGPs can be excluded at a 90 per cent level of certainty if $M_u \geq 1.138$ (Fisher *et al.* 1987; Tauxe 2010). The position of the palaeomagnetic pole before (R1) and after (R2) *E*/*I* correction is shown in panel (b). (c) The Q-Q analysis has been performed also on the combined Lainbach Valley data set, and also here the circular uniformity after *E*/*I* correction cannot be rejected at 90 per cent level of confidence. The L1 and L2 poles (same as Rehbrein Creek) are shown in (b). The R2 and L2 poles are compared with the reference European (E130) palaeomagnetic poles as described in the text. (d) Palaeogeographic reconstruction of the Alpine Tethys at Chron M0r (see the text for the rotational parameters used); Ap = Apulia platform, Br = Briançonnais terrain; Ib = Iblei platform, LiO = Ligurian Ocean, PiO = Piedmont Ocean; RDF = Rhenodanubian Flysch, Sa = Southern Alps and VaO = Valais Ocean. Question marks indicate a possible initiated subduction beneath the Adria–Africa margin, as suggested by Handy *et al.* (2010). The palaeolatitude of deposition for the RDF obtained from Rehbrein Creek (yellow triangles and line) and from Lainbach Valley (blue triangles and line) are shown together with the 95 per cent confidence boundary (small triangles).

there are no subchrons reported in the literature (Ogg *et al.* 2012). The short reverse interval at 13 and 14 m could have originated from sin- or post-depositional remagnetization processes. Similar 'excursions' have been found in the Cretaceous Scaglia facies of central Italy and interpreted as due to 'crypto-slumps', intrastrata movement of the sediments occurring in a early diagenetic phase (Cronin *et al.* 2001). Alternatively, they could be originated by geomagnetic excursion not recovered elsewhere. However, the robust correlation of our record with Chron M0, which constrains precisely the Barremian–Aptian boundary within the Rehbreingraben Formation, is not affected by the short reversal intervals retrieved upsection and their interpretation.

5.2 Palaeogeography of the RDF

At present, the palaeogeographic pertinence of the RDF has been determined only by geological evidences. These are mainly the position in the stacked Alpine nappes and the sediment type (Mattern 1999; Wortmann *et al.* 2001; Handy *et al.* 2010; Hesse 2011). In the frame of the Cretaceous palaeogeography, the RDF is commonly considered as deposited on the western margin of the Briançonnais terrane (Hesse 1973, 1974, 2011; Fig. 8c). Other authors proposed a strictly European pertinence of the RDF, suggesting a deposition on the northwestern flank of the Valais–Piedmont Ocean (Egger *et al.* 2002). Our palaeomagnetic data set gives the opportunity to locate the RDF in the frame of the Early Cretaceous Tethys using an independent geophysical constraint, that is, the palaeolatitude of deposition. The palaeomagnetic poles obtained from Rehbrein Creek (R) and Lainbach (L) are shown in Fig. 8(b). They have been calculated before (R1 and L1) and after (R2 and L2) correction for inclination shallowing of ChRM directions. Despite the facts that they plot on very similar colatitudes from the sampling site

Table 2. List of palaeomagnetic poles.

Pole	*N*	*K*	A_{95}	LONG	LAT
Hinterer Rehbrein Creek					
R1	133	18.0	3.0	160.0	52.2
R2	133	15.0	3.3	147.7	65.1
Lainbach Valley					
L1	87	34.7	2.6	171.2	65.0
L2	87	33.3	2.7	166.6	70.9

(62.2° and 60.1° for R2 and L2, respectively), we consider pole R2 more reliable. This is because we performed the *E*/*I* test at Rehbrein Creek using 133 directions, while at Lainbach the same routine has been applied on 87 directions. Tauxe *et al.* (2008) estimated a minimum number of ∼100–150 directions in order to obtain a reliable inclination shallowing correction, and only the data set from Rehbrein Creek falls in this range.

We compare poles R2 and L2 with the 130 Ma global synthetic palaeomagnetic pole of Torsvik *et al.* (2012), plotted in European coordinates (E130 pole). Even if the trajectories of the R2 and L2 poles with the associated A_{95} confidence boundaries cross to some extent the E130 pole, the absolute position indicates some amount of clockwise rotation of the sampling sites with respect stable Europe, as indicated in Fig. 8(b). The units pertaining to the Briançonnais and eastern European margin went through a Cretaceous dextral motion, with respect stable Adria–Africa, of several hundreds of kilometres, and this tectonic phase was followed by detachment, nappe stacking and uplift during the Cenozoic phase of the Alpine orogeny (Mattern 1999; Handy *et al.* 2010; Pfiffner 2014). Deviations of the palaeomagnetic declination of the RDF sediments from the reference European pole are thus expected. We plotted the palaeolatitude of deposition determined by the R2 and L2 palaeomagnetic poles on a palaeogeographic reconstruction of the Early Cretaceous Alpine Tethys, drawn using published data (Fig. 8d). We rotated the Africa–Adria block with respect stable Europe using the rotational parameter of Klitgord & Schouten (1986), while Iberia has been rotated following the rotation proposed by Olivet (1996). We then restored the palaeolatitudes of all domains placing the reconstruction on a palaeomagnetic reference frame by using the global synthetic 130 Ma pole of Torsvik *et al.* (2012). The main present-day coastal outlines are also shown for clarity. The eastward motion of the Iberian Plate with respect to stable Europe started as a consequence of the northward propagation of the Northern Atlantic Ocean spreading to the Bay of Biscay, and predates the magnetic anomaly M0r (Stampfli *et al.* 1998). It resulted in a total of ∼520 km sinistral strike-slip offset along the future Pyrenees (Handy *et al.* 2010, and reference therein). The eastward motion of Iberia may be coeval with the onset of the subduction of the Ligurian Ocean beneath the Africa–Adria active margin, as proposed by Handy *et al.* (2010). The transtensional rifting at the northern margin of Iberia triggered the opening of the Valais Ocean at the southeast European margin. It began at the Jurassic–Cretaceous boundary, resulting in a seafloor spreading that has lasted from ∼130 to ∼90 Ma (Liati *et al.* 2003; Handy *et al.* 2010). The Briançonnais terrain has been subsequently separated from the southern European margin by ∼100 km of oceanic crust. Considering that geological data indicate a southern origin of the sediments of the RDF (Hesse 1973, 2011), the palaeolatitude determined by the Rehbrein Creek data set (27.8° ± 3.3° N) is in agreement with a deposition of the RDF on the southwestern margin of the Briançonnais terrane, as proposed by Hesse (1973; see also Wortmann *et al.* 2001; Hesse 2011). The palaeolatitude determined from Lainbach Valley (29.9° ± 2.7° N) is shifted to the North by 2.1° with respect the one from Rehbrein Creek, but still in agreement with a Briançonnais pertinence of the RDF.

6 CONCLUSIONS

We conducted a palaeomagnetic study on the Lower Cretaceous Tristel Formation and Rehbreingraben Formation of the RDF (Eastern Alps). Successful results have been obtained in two localities, namely Rehbrein Creek and Lainbach Valley (Bavaria). Results from coeval sediments from the Falknis Nappe in Liechtenstein show that here the rocks are characterized by a pervasive synfolding remagnetization, hampering magnetostratigraphic or palaeogeographic interpretation. At Rehbrein Creek, we correlate two reverse polarity intervals of ∼1 and ∼0.25 m found within predominantly normal polarity with Chron M0r and with the M′-1r′event (or ISEA event, Ogg *et al.* 2012), resulting in an average sedimentation rate of 2.13 m Myr^{-1}. This correlation places the Barremian/Aptian boundary (126.3 Ma) within the base of the Rehbreingraben Formation. The estimated sedimentation rate of 2.13 is in good agreement with the ∼2.4 m Myr^{-1} proposed by Wortmann *et al.* (2004) using a ∂^{13}C-based correlation with reference curves. The high-quality palaeomagnetic data from Rehbrein Creek and Lainbach Valley, which pass either the reversal or the fold test, have been used to constrain the palaeogeographic position of the RDF within the evolving Alpine Tethys. Palaeomagnetic poles have been obtained with data corrected for inclination shallowing of ChRM directions, and the derived palaeolatitude of sedimentation help placing the RDF deposition across the Valais Ocean, on the western flank of the Briançonnais terrain, as proposed by Hesse (1973, 2011) and Wortmann *et al.* (2001). For the first time, reliable palaeomagnetic data are used to determine the age and the palaeogeographic pertinence of the RDF, an Alpine domain up to now constrained only by geological observation.

ACKNOWLEDGEMENTS

We thank Massimo Mattei and Roberto Molina for the comments that greatly improved the quality of the manuscript. We also thank Dario Bilardello for the fruitful discussion about the anisotropy of magnetic susceptibility analysis. This research has been supported by grants Ba1210/19-1,-2, and Da1757/1-1 of the Deutsche Forschungsgemeinschaft (DFG) to VB and ED.

REFERENCES

Anson, G.L. & Kodama, K.P., 1987. Compaction-induced inclination shallowing of the post-depositional remanent magnetization in a synthetic sediment, *Geophys. J. Int.,* **88,** 673–692.

Bouma, A.H., 1962. *Sedimentology of Some Flysch Deposits: A Graphic Approach to Facies Interpretation*, Elsevier, Amsterdam.

Channell, J.E.T., Erba, E., Muttoni, G. & Tremolada, F., 2000. Early Cretaceous magnetic stratigraphy in the APTICORE drill core and adjacent outcrop at Cismon (Southern Alps, Italy), and correlation to the proposed Barremian-Aptian boundary stratotype, *Bull. geol. Soc. Am.,* **112,** 1430–1443.

Cifelli, F., Mattei, M., Chadima, M., Hirt, A.M. & Hansen, A., 2005. The origin of tectonic lineation in extensional basins: combined neutron texture and magnetic analyses on "undeformed" clays, *Earth planet. Sci. Lett.,* **235,** 62–78.

Constable, C. & Tauxe, L., 1990. The bootstrap for magnetic susceptibility tensors, *J. geophys. Res.,* **95,** 8383–8395.

Cronin, M., Tauxe, L., Constable, C.G., Selkin, P. & Pick, T., 2001. Noise in the quiet zone, *Earth planet. Sci. Lett.,* **190,** 13–30.

Dallanave, E., Agnini, C., Muttoni, G. & Rio, D., 2009. Magnetobiostratigraphy of the Cicogna section (Italy): implications for the late Paleocene–early Eocene time scale, *Earth planet. Sci. Lett.,* **285,** 39–51.

Dallanave, E., Agnini, C., Muttoni, G. & Rio, D., 2012a. Paleocene magnetobiostratigraphy and climate-controlled rock magnetism from the Belluno Basin, Tethys Ocean, Italy, *Palaeogeog. Palaeoclimat. Palaeoecol.,* **337–338,** 130–142.

Dallanave, E., Muttoni, G., Agnini, C., Tauxe, L. & Rio, D., 2012b. Is there a normal magnetic-polarity event during the Palaeocene-Eocene thermal

maximum (~55 Ma)? Insights from the palaeomagnetic record of the Belluno Basin (Italy), *Geophys. J. Int.,* **191,** 517–529.
Egger, H., Homayoun, M. & Schnabel, W.G., 2002. Tectonic and climatic control of Paleogene sedimentation in the Rhenodanubian Flysch basin (eastern Alps, Austria), *Sediment. Geol.,* **152,** 247–262.
Enkin, R.J., 2003. The direction - correction tilt test: an all-purpose tilt/fold test for paleomagnetic studies, *Earth planet. Sci. Lett.,* **212,** 151–166.
Fisher, N.I., Lewis, T. & Embleton, B.J.J., 1987. *Statistical Analysis of Spherical Data*, Cambridge University Press, Cambridge, UK.
Fisher, R., 1953. Dispersion on a sphere, *Proc. R. Soc. A: Math. Phys. Eng. Sci.,* **A217,** 295–305.
Gradstein, F.M., Ogg, J.G., Schmitz, M.D. & Ogg, G.M., 2012. *The Geologic Time Scale 2012*, Elsevier, Amsterdam, Netherlands.
Handy, M.R., Schmid, S.M., Bousquet, R., Kissling, E. & Bernoulli, D., 2010. Reconciling plate-tectonic reconstructions of Alpine Tethys with the geological-geophysical record of spreading and subduction in the Alps, *Earth-Sci. Rev.,* **102,** 121–158.
Hesse, R., 1965. Herkunft und transport der sedimente im bayerischen flyschtrog, *Z. Dtsch. Geol. Gesellschaft,* **116,** 403–426.
Hesse, R., 1973. Flysch-Gault und Falknis-Tasna-Gault (Unterkreide): Kontinuierlicher Übergang von der distalen zur proximalen Flyschfazies auf einer penninischen Trogebene der Alpen, *Geol. Paleontol,* **SB2,** 1–90.
Hesse, R., 1974. Long-distance continuity of turbidites: possible evidence for an early cretaceous trench–abyssal plain in the east alps, Bull. geol. Soc. Am., **85,** 859–870.
Hesse, R., 1982. Cretaceous-Palaeogene flysch zone of the East Alps and Carpathians: identification and plate-tectonic significance of "dormant" and "active" deep-sea trenches in the Alpine-Carpathian Arc, in Leggett, J.K. Ed., *Trench-Forearc Geology*, Geological Society of London, Special Publication, Vol. 10, pp. 471–494.
Hesse, R. 2011. Rhenodanubian Flyschzone, Bavarian Alps, in *Geological Field Trips in Central Western Europe: Fragile Earth International Conference, Munich,* pp. 51–73, eds Carena, S., Friedrich, A.M. & Lammerer, B., Geological Society of America Field Guide 22.
Hirt, A.M., Banin, A. & Gehring, A.U., 1993. Thermal generation of ferromagnetic minerals from iron-enriched smectites, *Geophys. J. Int.,* **115,** 1161–1168.
Jelínek, V., 1978. Statistical processing of anisotropy of magnetic susceptibility measured on groups of specimens, *Stud. Geophys. Geod.,* **22,** 50–62.
Jelínek, V., 1981. Characterization of the magnetic fabric of rocks, *Tectonophysics,* **79,** T63–T67.
King, R.F., 1955. The remanent magnetism of artificially deposited sediments, *Monogr. Nat. R. Astron. Soc. Geophys. Suppl.,* **7,** 115–134.
Kirsch, K.-H., 2003. Dinoflagellatenzysten-Zonierung der höheren Unterkreide des Rhenodanubischen Flysches, *Zitteliana,* **A43,** 143–158.
Kirscher, U., Bilardello, D., Mikolaichuk, A. & Bachtadse, V., 2014. Correcting for inclination shallowing of early Carboniferous sedimentary rocks from Kyrgyzstan—indication of stable subtropical position of the North Tianshan Zone in the mid-late Palaeozoic, *Geophys. J. Int.,* **198,** 1000–1015.
Kirscher, U., Zwing, A., Alexeiev, D.V., Echtler, H.P. & Bachtadse, V., 2013. Paleomagnetism of Paleozoic sedimentary rocks from the Karatau Range, Southern Kazakhstan: multiple remagnetization events correlate with phases of deformation, *J. geophys. Res.,* **118,** 3871–3885.
Kirschvink, J.L., 1980. The least-squares line and plane and the analysis of palaeomagnetic data, *Geophys. J. Int.,* **62,** 699–718.
Klitgord, K.D & Schouten, H., 1986. Plate kinematics of the central Atlantic, in *The Geology of North America, The Western north Atlantic Region*, pp. 351–378. eds Vogt, P.R. & Tucholke, B.E. Geological Society of America, Boulder, CO.
Liati, A., Gebauer, D. & Fanning, C.M., 2003. The youngest basic oceanic magmatism in the Alps (Late Cretaceous; Chiavenna unit, Central Alps): geochronological constraints and geodynamic significance, *Contrib. Mineral. Petrol.,* **146,** 144–158.
Martín-Hernández, F., Luneburg, C.M., Aubourg, C. & Jackson, M., 2004. *Magnetic Fabric: Methods and Applications*, Vol. 238, Geological Society Special Publication, London.
Mattern, F., 1999. Mid-Cretaceous basin development, paleogeography, and paleogeodynamics of the western Rhenodanubian Flysch (Alps), *Z. Dtsch. Geol. Gesellschaft,* **150,** 89–132.
McElhinny, M.W. & McFadden, P.L., 1997. Palaeosecular variation over the past 5 Myr based on a new generalized database. *Geophys. J. Int.,* **131,** 240–252.
McFadden, P.L. & McElhinny, M.W., 1990. Classification of the reversal test in palaeomagnetism, *Geophys. J. Int.,* **103,** 725–729.
Ogg, J.G., Hinnov, L.A. & Huang, C., 2012. Cretaceous, *in The Geologic Time Scale*, pp. 793–853. eds Gradstein, F.M., Ogg, J.G., Schmitz, M.D. & Ogg, G.M., Elsevier.
Ogg, J.G., Hinnov, L.A. & Huang, C., 2012. Cretaceous, in Gradstein, F.M., Ogg, J.G., Schmitz, M.D. & Ogg, G.M., eds, *The Geologic Time Scale*, pp. 793–853. Elsevier.
Olivet, J.-L., 1996. La cinematique de la plaque Iberique, *Bull. des Centres Rech. Explor. Elf-Aquitaine,* **20,** 131–195.
Parés, J.M., van der Pluijm, B.A. & Dinarès-Turell, J., 1999. Evolution of magnetic fabrics during incipient deformation of mudrocks (Pyrenees, northern Spain), *Tectonophysics,* **307,** 1–14.
Pfiffner, A.O., 2014. *Geology of the Alps*, 2nd edn, Wiley Blackwell, Chichester, West Sussex, UK.
Stampfli, G.M., Mosar, J., Marquer, D., Marchant, R., Baudin, T. & Borel, G.D., 1998. Subduction and obduction processes in the Swiss Alps, *Tectonophysics,* **296,** 159–204.
Tan, X., Kodama, K.P. & Fang, D., 2002. Laboratory depositional and compaction-caused inclination errors carried by haematite and their implications in identifying inclination error of natural remanence in red beds, *Geophys. J. Int.*, **151,** 475–486.
Tarduno, J.A., 1990. Brief reversed polarity interval during the Cretaceous Normal Polarity Superchron, *Geology,* **18,** 683–686.
Tarduno, J.A., Sliter, W.V., Bralower, T.J., McWilliams, M., Premoli Silva, I. & Ogg, J.G., 1989. M-sequence reversals recorded in DSDP sediment cores from the western Mid-Pacific Mountains and Magellan Rise, *Bull. geol. Soc. Am.*, **101,** 1306–1316.
Tauxe, L., 2010. *Essentials of Paleomagnetism*, University of California Press, Berkeley.
Tauxe, L. & Kent, D.V., 1984. Properties of a detrital remanence carried by haematite from study of modern river deposits and laboratory redeposition experiments, *Geophys. J. Int.,* **77,** 543–561.
Tauxe, L. & Kent, D.V. 2004. A simplified statistical model for the geomagnetic field and the detection of shallow bias in paleomagnetic inclinations: was the ancient magnetic field dipolar?, in *Geophysical Monograph: Timescales of the Paleomagnetic Field* Vol. 145, pp. 101–115, eds Channell, J.E.T., Kent, D.V., Lowrie, W. & Meert, J.G. American Geophysical Union, Washington, DC.
Tauxe, L., Kodama, K.P. & Kent, D.V., 2008. Testing corrections for paleomagnetic inclination error in sedimentary rocks: a comparative approach, *Phys. Earth planet. Inter.,* **169,** 152–165.
Tauxe, L. *et al.* 2016. PmagPy: software package for paleomagnetic data analysis and a bridge to the Magnetics Information Consortium (MagIC) Database, *Geochem. Geophys. Geosyst.,* **17,** 2450–2463.
Torsvik, T.H. *et al.* 2012. Phanerozoic polar wander, palaeogeography and dynamics, *Earth-Sci. Rev.,* **114,** 325–368.
Vandenberg, J., Klootwijk, C.T. & Wonders, A.A.H., 1978. Late Mesozoic and Cenozoic movements of the Italian peninsula: Further paleomagnetic data from the Umbrian sequence, *Geol. Soc. Am. Bull,* **89,** 133–150.
Wagreich, M., Pavlishina, P. & Malata, E., 2006. Biostratigraphy of the lower red shale interval in the Rhenodanubian Flysch Zone of Austria, *Cretaceous Res.,* **27,** 743–753.
Wang, L., Pan, Y., Li, J. & Qin, H., 2008. Magnetic properties related to thermal treatment of pyrite, *Sci. China Ser. D—Earth Sci.,* **51,** 1144–1153.
Watson, G., 1983. Large sample theory of the Langevin distribution, *J. Stat. Plan. Infer.,* **8,** 245–256.
Watson, G.S. & Enkin, R.J., 1993. The fold test in paleomagnetism as a parameter estimation problem, *Geophys. Res. Lett.,* **20,** 2135–2137.

Wortmann, U.G., Herrle, J.O. & Weissert, H., 2004. Altered carbon cycling and coupled changes in Early Cretaceous weathering patterns: evidence from integrated carbon isotope and sandstone records of the western Tethys, *Earth planet. Sci. Lett.,* **220,** 69–82.

Wortmann, U.G., Hesse, R. & Zacher, W., 1999. Major-element analysis of cyclic black shales: paleoceanographic implications for the Early Cretaceous deep western tethys, *Paleoceanography,* **14,** 525–541.

Wortmann, U.G., Weissert, H., Funk, H. & Hauck, J., 2001. Alpine plate kinematics revisited: the Adria Problem, *Tectonics,* **20,** 134–147.

Zhu, R., Hoffman, K.A., Nomade, S., Renne, P.R., Shi, R., Pan, Y. & Shi, G., 2004. Geomagnetic paleointensity and direct age determination of the ISEA (M0r?) chron, *Earth planet. Sci. Lett.,* **217,** 285–295.

Zijderveld, J.D.A., 1967. A.C. demagnetization of rocks: analysis of results, in *Methods in Paleomagnetism*, pp. 254–286, eds Collinson, D.W., Creer, K.M. & Runcorn, S.K., Elsevier, New York.

SUPPORTING INFORMATION

Supplementary data are available at *GJI* online.

Table S1. Anisotropy of magnetic susceptibility measurements and derived parameters for Rehbrein Creek and Lainbach Valley. Dec. and Inc. = Declination and inclination. L, F, $P$and T = lineation, foliation, corrected anisotropy degree and shape factor (Jelínek 1981); ζ and η = semi-angles of the confidence ellipses (Constable & Tauxe 1990).

Please note: Oxford University Press is not responsible for the content or functionality of any supporting materials supplied by the authors. Any queries (other than missing material) should be directed to the corresponding author for the paper.